P H Y S I C A L   R E V I E W   L E T T E R S

Integer Quantum Hall Effect on a Six-Valley Hydrogen-Passivated Silicon (111) Surface

K. Eng, R. N. McFarland, and B. E. Kane

Laboratory for Physical Sciences, University of Maryland at College Park, College Park, Maryland 20740, USA
(Received 9 April 2007; published 5 July 2007)

We report magnetotransport studies of a two-dimensional electron system formed in an inversion layer at the interface between a hydrogen-passivated Si(111) surface and vacuum. Measurements in the integer quantum Hall regime demonstrate that the expected sixfold valley degeneracy for these surfaces is broken, resulting in an unequal occupation of the six valleys and anisotropy in the resistance. We hypothesize the misorientation of Si surface breaks the valley states into three unequally spaced pairs, but the observation of odd filling factors is difficult to reconcile with noninteracting electron theory.

The silicon field effect transistors (FETs) that are at the heart of contemporary microelectronics rely on mobile electrons or holes confined at the interface between Si and a higher band gap barrier material. This barrier in metal oxide silicon (MOS) FETs is SiO_2, an amorphous material which introduces inevitable disorder at the Si-SiO_2 interface and limits the carrier mobility in these devices. A crystalline interface can be created using epitaxial SiGe-Si layers in which mobilities can be over an order of magnitude higher than the best MOSFET devices [1], but this technique is limited to the [100] oriented surfaces [2]. Recently, a new technique for Si crystalline interfaces has been demonstrated [3] in which a Si interface is passivated with a monolayer of hydrogen and the barrier material is a vacuum. While the inertness and high degree of atomic perfection of these surfaces has been known for some time [4−6], the development of high mobility electronic devices on H-Si enables the exploration of two-dimensional (2D) physics of novel Si surface orientations and may one day allow quantum devices to be engineered at the atomic scale using surface manipulation techniques [7].

We report here the first detailed magnetotransport studies of a 2D electron system (2DES) at a H-Si(111) surface gated through a vacuum barrier. Electron mobilities are an order of magnitude higher (24,000 $cm^2/V s$) than Si(111) MOSFETs, enabling the observations of the integer quantum Hall effect (IQHE). In the effective mass approximation, the ground state for a 2DES on the Si(111) surface is sixfold degenerate with each Si conduction band valley contributing an equal number of carriers [Fig. 1(d)], each with anisotropic in-plane masses, $m_x = 0.19 m_o$ and $m_y = 0.67 m_o$ [8] (m_o is the mass of the free electron). However, measurements of Shubnikov−de Haas (SdH) oscillations in Si(111) MOSFETs have shown conflicting valley degeneracies of two [8–10] and six [11,12] along with isotropic resistivities for both. Subsequent proposals [11,13] have tried to explain these anomalous observations, but to date, conclusive experimental results are still lacking.

The high mobility 2DES can be created by contact bonding two individual Si substrates [3] [Fig. 1(a)]. One

is the H-Si(111) substrate (float zone, p-type, $\rho \sim 10 \, \Omega \, cm$) which has four phosphorous contacts forming a 1-mm-wide square with sides oriented parallel to the $[1\bar{1}0]$ and $[11\bar{2}]$ crystallographic directions [Fig. 1(b) and 1(c)]. The second is a silicon-on-insulator (SOI) substrate which acts as the remote gate, where an electric field can be controlled within an etched cavity. The Si(111) surface is H-passivated by immersion in an ammonium fluoride solution. The two substrates are then bonded in vacuum ($\sim 10^{-6}$ Torr), which allows the remote gate to
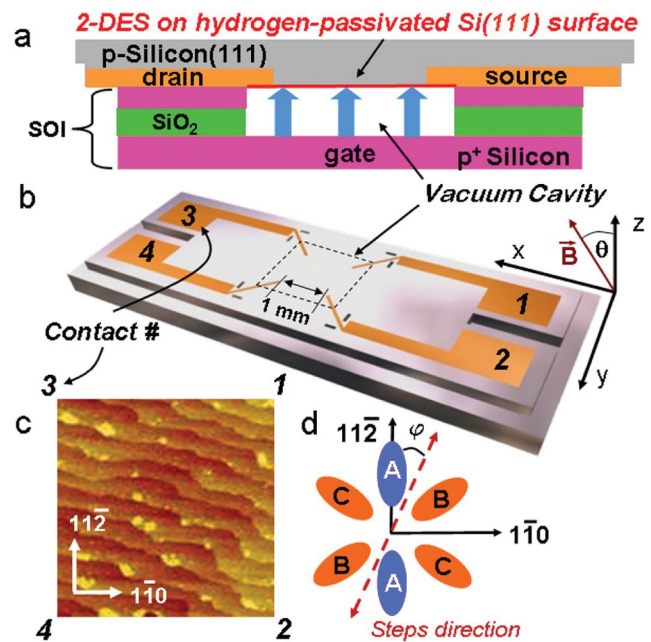

FIG. 1 (color). (a) Schematic cross-section of a H-Si(111) substrate contact bonded to a SOI substrate. A p^+ layer in the SOI defines the gate, where blue arrows depict the electric field. A 2DES is formed at the H-Si(111) surface within an encapsulated cavity. (b) The H-Si(111) substrate has four n^+ contacts numbered accordingly. Tilted magnetic fields are applied in the x-z plane. (c) A 1 μm $\times$ 1 μm AFM image of atomic steps on a H-Si(111) surface in relation to the crystal directions and the contacts of the device. (d) The projection of the six valleys for the Si(111) surface with pairs of valleys labeled A, B, and C.

induce electrons on the H-Si(111) surface and protects the air sensitive surface inside the cavity.

Figure 2(a) shows traces of the Hall (R_{xy}) and the longitudinal resistance (R_{xx}) as a function of perpendicular magnetic field, $B_\perp$, for a constant electron density, $n = 6.5 \times 10^{11}$ cm^{-2} at $T = 300$ mK. We have obtained similar data in two devices over a wide range of n. We present data for a single device at a density where IQHE features are most apparent. There are two orientations in which R_{xx} is measured: $R_{(12,34)}$ and $R_{(13,24)}$, where the first and second subscripts represent the current and voltage contacts, respectively [Fig. 1(b)]. Anisotropy in R_{xx} is observed, but both orientations exhibit minima that occur at integer values of filling factor, $\nu = nh/eB_\perp$. Similar behavior (within 3%) is also observed for $R_{(43,21)}$ and $R_{(42,31)}$. These minima are directly correlated with the observed plateaus in R_{xy}, a trademark of the QHE. Filling factors less than six are observed at $\nu = 5$, 4, 3, and 2, where $\nu =$
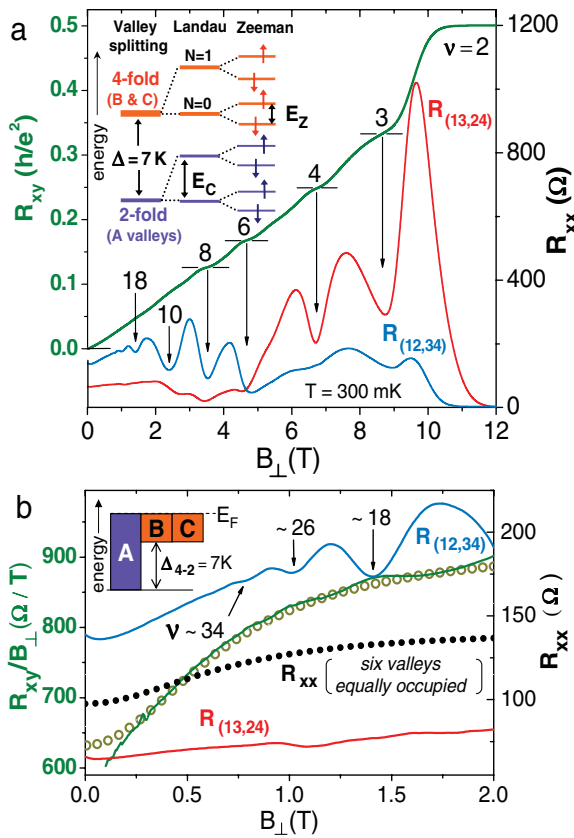
5 is apparent through $d^2R_{xx}/dB_\perp^2$. Figure 2(b) shows characteristic behavior at low B fields: $R_{xy}/B_\perp$ is dependent on $B_\perp$; both $R_{(12,34)}$ and $R_{(13,24)}$ display a positive magnetoresistance (MR); finally, while more apparent in $R_{(12,34)}$, both orientations display SdH oscillations with minima occurring approximately every eighth Landau level (LL) filling factor, $\Delta\nu \sim 8$.

Classical MR calculations [14] show that in a multicomponent electron system in which electrons have differing anisotropic in-plane masses, R_{xy} is nonlinear with respect to $B_\perp$, and R_{xx} should display a positive MR. In Fig. 2(b), we plot $R_{xy}/B_\perp$ and $R_{xx}(B)$ overlaid with a classical MR model in which all six valleys are equally occupied, with n and the mean scattering time, τ, as free parameters. The values which provided the best fit to R_{xy} are within 5% of observed values: $\tau = 3.5$ ps and $n \simeq 6.8 \times 10^{11}$ cm^{-2}. This model agrees well with the observed behavior in R_{xy} and the positive MR in R_{xx}. However, in order to explain the observed anisotropy in R_{xx}, an unequal population of electrons among the six valleys is required.

The strong R_{xx} minimum at $\nu = 2$, suggests a gap between the six valleys. We obtain gap energies, Δ_ν, from the temperature dependence of R_{xx}, $R_{xx} \sim \exp(-\Delta_\nu/2k_BT)$. These measurements show that the energy gap, Δ_2, is insensitive to small changes in $B_\perp$ and in-plane fields, $B_\parallel$ (Table I). It is by far the largest gap ($\simeq$ 7 K) and provides strong evidence that the six valleys are indeed broken asymmetrically following a 4-2 valley configuration. For simplicity, we will assume a model which is composed of only one type of splitting which is independent of B: two valleys (A) are 7 K lower in energy than the remaining four valleys (B and C) in the ground state [inset of Fig. 2(b)]. The inset of Fig. 2(a) illustrates the effect $B_\perp$ has on the density of states, $\mathcal{D}(E)$, for this "7 K model." Quantization of the electron's orbital motion creates LLs which are separated by the cyclotron gap, $E_C = \hbar eB_\perp/m_\mathcal{D}$, where $m_\mathcal{D} = (m_x m_y)^{1/2} = 0.358m_o$ is the density of states mass for Si(111). Each LL then splits into two energy levels due to spin. This energy separation is the Zeeman energy, $E_Z = g^*\mu_BB_\perp/\cos\theta$, where g^* is the effective g-factor and μ_B is the Bohr magneton.

The validity of this 7 K model can be tested with measurements in R_{xx} versus tilted B fields. Rotating the device some angle, θ, away from $B_\perp$ changes E_Z with respect to E_C, and eventually energy levels of different

FIG. 2 (color).   (a) R_{xy} (green), $R_{(12,34)}$ (blue), and $R_{(13,24)}$ (red) versus $B_\perp$ for the device at $T = 300$ mK and $n = 6.5 \times 10^{11}$ cm^{-2}. Plateaus in R_{xy} are labeled by horizontal bars, and the numbers indicate their corresponding filling factor ν. The inset is a schematic energy level diagram depicting the three energy scales affecting $\mathcal{D}(E)$ at $B_\perp = 1$ T. (b) The same data from (a) are plotted within $0 \le B_\perp \le 2$ T. Hall resistance is plotted as $R_{xy}/B_\perp$, and the divergence is removed for $B_\perp \le$ 0.1 T. Open symbols ($R_{xy}/B_\perp$) and closed symbols (R_{xx}) correspond to calculations having all six valleys equally occupied. The inset depicts $\mathcal{D}(E)$ for the 7 K model at $B = 0$.

TABLE I.   Energy gaps for various filling factors, where $\theta = 0°$ corresponds to a magnetic field normal to the 2DES. The subscripts in $\Delta_{(12,34)}$ represent the measurement orientation.

ν	n ($\times 10^{11}$ cm^{-2})	θ	$\Delta_{(13,24)}$ (K)	$\Delta_{(12,34)}$ (K)
2	5.69	0°	8 ± 0.5	7 ± 0.5
3	6.50	39°	0.4 ± 0.2	0.8 ± 0.2
4	6.50	48.4°	1.1 ± 0.2	1.2 ± 0.2
6	6.50	48.4°	1.1 ± 0.2	1.2 ± 0.2

spins will overlap with one another. The angles at which these coincidences occur can be observed through the disappearance of minima in R_{xx}. One such coincidence is shown in Fig. 3(a), where a minimum in $d^2R_{(12,34)}/dB_\perp^2$ corresponds to the disappearance of the R_{xx} minimum at $\nu = 8$ and a concomitant maximum occurs at $\nu = 10$. Similar behavior is also observed for $d^2R_{(13,24)}/dB_\perp^2$. The second derivatives of R_{xx} are plotted in order to amplify structure and to eliminate the contribution from the positive MR at low B fields. Figure 3(b) depicts a schematic energy level diagram following the 7 K model and using $B_\perp$ values centered at $\nu = 8$. The 7 K model identifies this
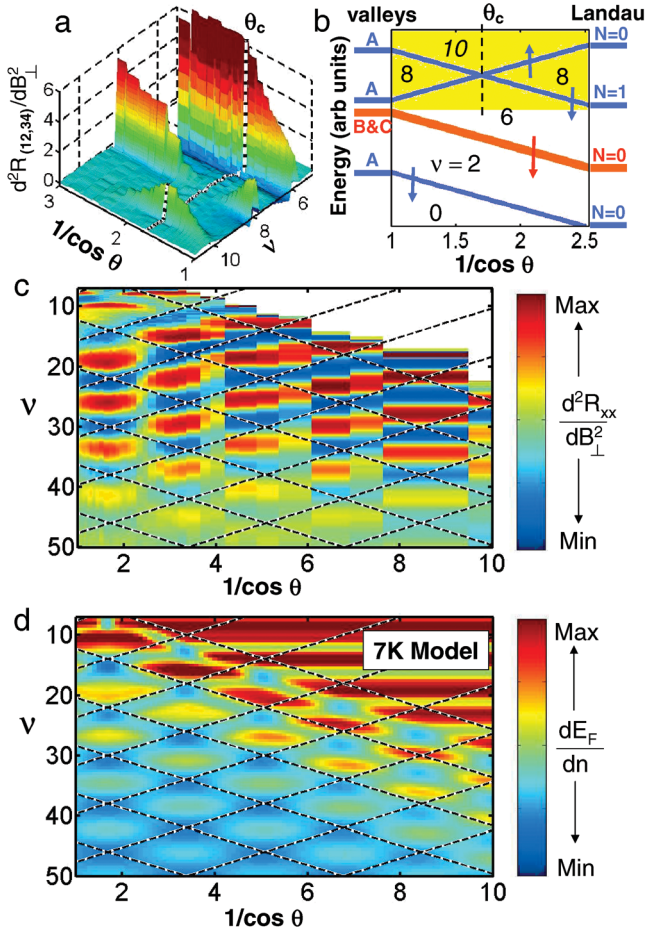

FIG. 3 (color). Data and calculations represented at $n = 6.5 \times 10^{11}$ cm^{-2} and $T = 300$ mK. For the color scales represented in (a), (c), and, (d), a maximum in $d^2R_{xx}/dB_\perp^2$ or dE_F/dn corresponds to a minimum in R_{xx}. (a) A surface plot of $d^2R_{(12,34)}/d\nu^2$ versus $1/\cos\theta$ for filling factors within $5 \leq \nu \leq 11$. At θ_c, the R_{xx} minimum at $\nu = 8$ disappears while a minimum at $\nu = 10$ is at a peak. (b) Schematic energy level diagram following the 7 K model predicting the twofold energy levels from the A valleys (spin up and spin down) crossing one another at θ_c. (c) A plot of $d^2R_{(12,34)}/dB_\perp^2$ versus ν and $1/\cos\theta$. The overlaid schematic fan diagram (dashed lines) represents expectations from the 7 K model with $\Delta\nu \simeq 8$. (d) A plot of a calculated dE_F/dn versus ν and $1/\cos\theta$ using the 7 K model. The same fan diagram used in (c) is overlaid on top of calculations.

observed behavior with a crossing between the two-fold degenerate A valleys in the upper spin level of the lowest LL ($N = 0$) and the lowest spin level of the second LL ($N = 1$). This crossing occurs when $E_Z = E_C$. Assuming the effective mass equals $m_D = 0.358m_o$, we obtain an enhanced $g^* = 3.3$ (bare value $g = 2$). When these parameters are used, the 7 K model can explain the observed strengthening of the $\nu = 6$ minimum with increasing θ prior to the level crossing and, although not shown, explains why $\nu = 12$ is never observed.

The 7 K model with $m_D = 0.358m_o$ implies $\sim$50% of the electrons are occupying the lowest two valleys at small B fields. If only these contributed to the low B SdH oscillations, a periodicity of $\Delta\nu \simeq 8$ would be expected if the degeneracy due to spin and valley pairs with opposite **k** remain unresolved. Figure 3(c) shows the remainder of the coincidence measurements, where $d^2R_{(12,34)}/dB_\perp^2$ is plotted versus $1/\cos\theta$ (x axis) and ν (y axis). The plot is a compilation of $R_{(12,34)}$ measurements oriented at 45 different θ's, and evidence of up to $\sim$5 level crossings is apparent. A schematic energy fan diagram in accordance with expectations from the 7 K model, $\Delta\nu = 8$ and $g^* = 3.3$, is overlaid on top of the data, and the intersections of the levels coincides with minima in $d^2R_{(12,34)}/dB_\perp^2$ or maxima in R_{xx}. Figure 3(d) shows calculations derived from the 7 K model of the derivative of the Fermi energy with respect to the density, dE_F/dn, in the same range plotted in Fig. 3(c). The same fan diagram used in Fig. 3(c) is also overlaid on top of the calculations. By applying different Dingle temperatures, 0.6 K and 2 K, to the carriers originating from the twofold and fourfold valleys, respectively, the 7 K model is able to reproduce the unresolved spin degeneracy and the absence of oscillations from the higher energy valleys seen in the data. Differing scattering times are commonly observed in two component electron systems with different densities [15].

A likely origin for breaking the valley degeneracy in our 2DES is the miscut of the wafer. This miscut angle, ψ, can be derived from the width of the atomic steps on a H-Si(111) surface. Figure 1(b) shows an atomic force microscope (AFM) image of a H-Si(111) surface obtained from an adjacent piece of the Si(111) wafer used to fabricate the device. From the AFM image, we observe steps running at an angle, $\phi \simeq 15 \pm 5°$, off from the $[11\bar{2}]$ axis with an average width of $\sim$90 nm. This corresponds to a miscut of $\psi \sim 0.2°$ and is approximately about the $[1\bar{1}0]$ axis. In the effective mass approximation, this miscut increases the normal mass, m_z, of the two valleys (A) aligned with the $[11\bar{2}]$ direction by $\sim$0.5% relative to the remaining four valleys (B and C). As a result, the sixfold symmetry is broken into a 4-2 valley configuration similar to our 7 K model, but with an energy gap of only $\Delta_{4-2} \sim 2$ K. Additionally, the four valleys (B and C) occupied at higher energies are split due to the off axis rotation of ϕ. This energy gap is calculated to be much smaller, $\Delta_4 \sim 0.2$ K, which is within our experimental uncertainties, but poten-
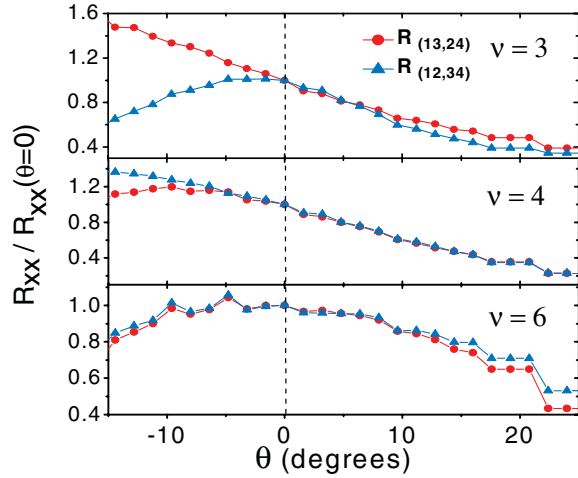
PHYSICAL REVIEW LETTERS

FIG. 4 (color). R_{xx} minima at $\nu = 3$, 4, and 6 are divided by their respective R_{xx} values at $\theta = 0°$ and plotted within $-15° \leq \theta \leq 25°$. Data represent measurements at $T = 300$ mK and $n = 6.5 \times 10^{11}$ cm^{-2}.

tially explains the presence of $\nu = 4$. It is possible that the discrepancy in the magnitude of Δ_2 is due to a many-body enhancement. However, these predicted energy gaps do not include possible effects the atomic steps at the surface may have on the confinement of the electronic wave function [16].

The simple 7 K model does break down at high B, specifically for the observed minima at $\nu = 5$, 4, and 3. Figure 4 displays the behavior of the R_{xx} minima for $\nu = 6$, 4, and 3 versus small θ. In agreement with the 7 K model, the $\nu = 6$ minimum strengthens as $\sim 1/\cos\theta$ for small positive and negative tilts about $\theta = 0°$. However, the R_{xx} minima for $\nu = 4$ are observed to have a linear response to small tilts about $B_\perp$. For surface electrons which have nonzero off diagonal terms normal to the surface in the effective mass tensor, it is possible to have confinement energies depending linearly on θ [17]. The magnitude of this effect is $\propto \sin\theta \cos\theta$ and has a peak value of ~ 1.5 K for $\nu = 4$. This agrees well with the observed linear response around small θ for $\nu = 4$.

The observation of $\nu = 3$ and 5 indicates that the in-plane symmetry of $\pm\mathbf{k}_\parallel$ between opposite valleys is broken on our H-Si(111) surface. We also observe $\nu = 3$ to be the only state which exhibits anisotropy in Δ between the two resistance orientations (Table I). Figure 4 shows that this anisotropy is also dependent on the measurement orientation with respect to $B_\parallel$. This splitting cannot be explained by uniform strain or misorientation effects in the effective mass approximation. It also cannot be easily interpreted using theories developed for valley splittings on [100] Si surfaces [8,16], where the confinement potential couples valleys with minima in the direction normal to the surface. It is possible that disorder on the surface couples the opposite $\mathbf{k}_\parallel$ valleys in our samples. However, anisotropies of R_{xx} developing at low temperatures are also observed in

other high mobility 2D systems [18,19] and have been attributed to correlated electron phases. The physics may also be similar to the lifting of the sublattice symmetry recently observed in graphene [20], or to skyrmion states in multivalley electron systems [21,22].

We note that our sample fabrication process is not yet optimized and that prospects for substantially improved mobilities are good. Our results imply that the valley splitting on the Si(111) surfaces can be tuned by wafer orientation and in-plane magnetic fields. Thus, H-passivated Si surfaces can be prepared with the maximum number of valley degrees of freedom in which to explore potentially new many-body quantum phenomena, such as exotic fractional quantum Hall states [23], and "valley singlet" states which are potentially relevant for topological quantum computing [24]. Lastly, the relative ease of incorporating surface engineering within the fabrication process may enable future experiments in which high mobility electrons are coupled to molecules or atoms on an atomically clean semiconductor surface.

[1] F. Schäffler, Semicond. Sci. Technol. **12**, 1515 (1997).
[2] M. L. Lee *et al.*, Thin Solid Films **508**, 136 (2006).
[3] K. Eng, R. N. McFarland, and B. E. Kane, Appl. Phys. Lett. **87**, 052106 (2005).
[4] G. S. Higashi *et al.*, Appl. Phys. Lett. **56**, 656 (1990).
[5] E. Yablonovitch *et al.*, Phys. Rev. Lett. **57**, 249 (1986).
[6] M. Hines, Annu. Rev. Phys. Chem. **54**, 29 (2003).
[7] J. L. O'Brien *et al.*, Phys. Rev. B **64**, 161401(R) (2001).
[8] T. Ando, A. B. Fowler, and F. Stern, Rev. Mod. Phys. **54**, 437 (1982).
[9] D. C. Tsui and G. Kaminsky, Solid State Commun. **20**, 93 (1976).
[10] G. Dorda, I. Eisele, and H. Gesch, Phys. Rev. B **17**, 1785 (1978).
[11] D. C. Tsui and G. Kaminsky, Phys. Rev. Lett. **42**, 595 (1979).
[12] T. Cole and B. D. McCombe, Phys. Rev. B **29**, 3180 (1984).
[13] M. J. Kelly and L. M. Falicov, Phys. Rev. Lett. **37**, 1021 (1976).
[14] R. A. Smith, *Semiconductors* (Cambridge University Press, Cambridge, England, 1978), Chap. 5.
[15] H. van Houten *et al.*, Phys. Rev. B **37**, 2756(R) (1988).
[16] M. Friesen, M. A. Eriksson, and S. N. Coppersmith, Appl. Phys. Lett. **89**, 202106 (2006).
[17] F. Stern and W. E. Howard, Phys. Rev. **163**, 816 (1967).
[18] M. P. Lilly *et al.*, Phys. Rev. Lett. **82**, 394 (1999).
[19] W. Pan *et al.*, Phys. Rev. B **64**, 121305(R) (2001).
[20] Y. Zhang *et al.*, Phys. Rev. Lett. **96**, 136806 (2006).
[21] M. Shayegan *et al.*, Phys. Status Solidi B **243**, 3629 (2006).
[22] D. P. Arovas, A. Karlhede, and D. Lilliehöök, Phys. Rev. B **59**, 13147 (1999).
[23] K. Lai *et al.*, Phys. Rev. Lett. **93**, 156805 (2004).
[24] E. Ardonne and K. Schoutens, Ann. Phys. (N.Y.) **322**, 201 (2007).